Available online at www.sciencedirect.com
ScienceDirect
Journal of the European Ceramic Society 31 (2011) 687–695
www.elsevier.com/locate/jeurceramsoc

Sintering and characterization of flyash-based mullite with MgO addition

Yingchao Dong [a,b,c,*], Stuart Hampshire [a,**], Jian-er Zhou [b], Zhanlin Ji [a], Jiandong Wang [b], Guangyao Meng [c]

[a] *Materials and Surface Science Institute (MSSI), University of Limerick, Limerick, Ireland*
[b] *Key Lab of Jiangxi Universities for Inorganic Membranes, Jingdezhen Ceramic University (JCU), PR China*
[c] *USTC Lab for Solid State Chemistry and Inorganic Membranes, University of Science and Technology of China (USTC), PR China*

Received 29 September 2010; received in revised form 1 December 2010; accepted 7 December 2010
Available online 6 January 2011

Abstract

Mullite ceramics were fabricated at relatively low sintering temperatures (1500–1550 °C) from recycled flyash and bauxite with MgO addition as raw materials. The densification behavior was investigated as function of magnesia content and sintering temperature. The results of thermal analysis, bulk density and pore structure indicate that MgO addition effectively promoted sintering, especially above 1450 °C. Due to the presence of large interlocked elongated mullite crystals above 1450 °C, associated with enhanced densification, an improvement in mechanical strength was obtained for the samples containing magnesia. The addition of magnesia slightly decreases the LTEC at 1300 °C due to the formation of low-expansion α-cordierite, but slightly increases the LTEC above 1400 °C due to the formation of high expansion corundum and $MgAl_2O_4$ spinel.

Keywords: Flyash; Environmental application; Mullite; Sintering; Magnesia

1. Introduction

In recent years, there has been considerable increasing interest in environmental problems worldwide. In particular, many researchers have concentrated more attention on seeking sustainable methods for recycling of hazardous industrial wastes. As an abundant waste, coal flyash is a by-product derived from raw coal combustion in thermal power plants and factories which presents many countries with serious problems of storage and environmental pollution but it can be considered as the world's fifth largest raw material resource.[1] Research activities relating to the utilization of flyash have resulted in various applications, mainly in the construction sector (cement and concrete),[2] agriculture sector (soil amendment) and advanced materials such as mineral polymers, synthetic zeolite, glass, glass–ceramics, porous ceramics and composite catalysts.[3] In many cases, the chemical and phase compositions of flyash are complex, depending on raw coal and combustion conditions.[4] In spite of its diversity, flyash is rich in certain metal oxides such as silica (SiO_2) and alumina (Al_2O_3). This gives flyash the potential to be used as a low cost material source for the glass and ceramic industries. The effective utilization of waste flyash not only resolves a huge environmental issue, but also produces high value-added materials while conserving natural resources.

Mullite is a strong candidate ceramic for advanced structural applications at high temperatures, because it has a high melting point, good creep resistance, superior high temperature strength, exceptional thermal shock resistance and exhibits good chemical stability in harsh chemical environments. Amongst the potential applications are thermal and environmental barrier coatings for aircraft and gas turbine engines, catalytic converters, kiln furniture and hot gas filters/membranes, 3:2 mullite has a highly stable open structure and it can accommodate transition metal cations into its structure.[5] Flyash, in which SiO_2 and Al_2O_3 are its main components, is very suitable to produce mullite because it contains large amounts of reactive SiO_2 and alumina.[6] Recently, some researchers have attempted to prepare mullite from this waste with addition of industrial α-alumina.[7–10] In our previous work,[11] a dense 3:2 mullite was synthesized from flyash with addition of raw bauxite as alumina source. A unique vol-

* Corresponding author at: Materials and Surface Science Institute, University of Limerick, Limerick, Ireland. Tel.: +353 61202640; fax: +353 61338172.
** Corresponding author. Tel.: +353 61202640; fax: +353 61338172.
E-mail addresses: yingchao.dong@ul.ie (Y. Dong), stuart.hampshire@ul.ie (S. Hampshire).

0955-2219/$ – see front matter © 2010 Elsevier Ltd. All rights reserved.
doi:10.1016/j.jeurceramsoc.2010.12.012

ume expansion occurred at 1380–1520 °C, resulting in a highly porous microstructure. In order to obtain dense mullite, therefore, it is necessary to commence densification before expansion.

The use of sintering aids is a quite important strategy in reduction of sintering temperatures for pure mullite. Some oxides such as titania, ferric oxide, strontia, ceria and YSZ (yttrium stabilized zirconia) have been very effective in promoting densification.[12–14] MgO has been used as an effective aid to lower sintering temperature of industrial mullite[12,15,16] and combustion processed mullite.[17] Nevertheless, most of the past research has focused on low-temperature densification of pure mullite. Little attention has been paid to the effect of MgO addition on the properties of reaction-sintered mullite made from recycled materials.

In the current work, reaction-sintered 3:2 mullite was prepared from two recycled materials, i.e., waste flyash and natural bauxite, with MgO as sintering aid. The effects of MgO content and sintering temperature on sintering behavior, mechanical and thermal properties, phase composition and microstructure were studied in detail.

2. Experimental procedure

2.1. Starting materials, pressing and sintering

Flyash (Hefei No. 2 thermal power plant, PR China) and natural bauxite (Yangquan City, PR China) powders were used as the main starting materials to prepare mineral-based mullite.[11] Basic magnesium carbonate (AR; $(MgCO_3)_4{\cdot}Mg(OH)_2{\cdot}5H_2O$; Sinopharm Chemical Reagent Co., Ltd.) was used as the magnesia source for the sintering additive. The mixture of flyash and bauxite, based on the composition of 3:2 mullite (W_{flyash}:$W_{bauxite}$ = 45.87:100), was wet-mixed for 6 h using zirconia balls with distilled water as medium in a polyethylene pot. The average particle diameters of flyash, bauxite and their mixture are 1.76, 1.13 and 1.52 μm. For the mixture, most of the particles center at 1.00–4.00 μm in diameter.

After wet-mixing, basic magnesium carbonate was added and the agitation was continued unceasingly for 2 h using a mechanical stirrer. Then, the slurry of mixed powders was completely dried at 120 °C. Afterwards, the mixture was slightly crushed to break the agglomerates, mixed with binder PVA-1750 (5.00 wt.%) and then uniaxially pressed at 160 MPa. Both rectangular bars (50 mm × 6 mm × 3–4 mm) and cylindrical pellets (25 mm in diameter; 2–3 mm in height) were made. After sufficient drying at 120 °C, the samples were fired between 1300 and 1500 °C at intervals of 50 °C for 2 h dwelling time. The heating rates were 1 °C min^{-1} from room temperature to 450 °C, 2 °C min^{-1} from 450 to 650 °C, and 3 °C min^{-1} from 650 °C to the final firing temperatures. A dwelling time of 1 h was carried out at 450 and 650 °C, respectively, to remove added organic additives and inherent structural water in natural bauxite.

2.2. Characterization techniques

The particle size distributions of flyash, bauxite and their mixture were determined using a laser particle size analyzer (Rise-2006, Jinan Rise Science & Technology Co. Ltd., PR China) using PEG-10000 (polyethylene glycol; molecular weight: 10,000 g mol^{-1}) as dispersing agent. Sintering shrinkage behavior of the green bodies containing various magnesia contents was measured between 26 °C and 1550 °C at a heating rate of 3 °C min^{-1} in a horizontal dilatometer (DIL 402C, Netzsch, Germany).

Linear dimensional changes in the diameters of the sintered pellets were measured using a vernier caliper. In addition, both bulk density and open porosity were measured in distilled water using the Archimedes' replacement method. Pore size distributions were examined in a lab-made equipment according to the bubble point method, which is on the basis of gas–liquid replacement mechanism.[18]

Room temperature flexural strength was determined by the three-point bending method in a universal materials testing machine (3369, Instron Corporation, USA). A span length of 30 mm and crosshead speed of 0.5 mm min^{-1} were used. All the tested bars were polished and beveled in advance by 360-mesh and then 800-mesh metallographic sandpapers in order to eliminate surface stress. Fracture strength was calculated according to the following expression (ISO9693 1999).

$$\sigma = \frac{3P \times l}{2b \times h^2}$$

where σ is fracture strength (Pa), P is fracture load (N), l is span length (m), b is sample width (m), h is sample height (m).

Fracture surfaces of the sintered bodies were observed using FE-SEM (Field Emission Scanning Electronic Microscope; JSM-6700F, JEOL, Japan). EDS micro-region analysis (INCA300, Oxford Instrument, England) was carried out on 4 randomly selected positions in the fracture surfaces of the samples with and without 4 wt.% MgO after washing with 15 vol.% HF solution for 20 min and then drying at 120 °C.

The linear thermal expansion coefficients (LTEC) of the sintered samples were measured in a horizontal dilatometer over the temperature range of 25–1000 °C at a heating rate of 10 °C/min. The sintered discs were characterized using XRD (Cu Kα radiation; D8 ADVANCE, Bruker Corporation, Germany) to determine the final phase assemblage.

3. Results and discussion

3.1. Sintering behaviors with different magnesia contents

3.1.1. Dilatometric measurement

Fig. 1 displays the sintering behavior of the flyash-based mullite with 0–4 wt.% MgO. The sample without MgO exhibits low shrinkages at all temperatures, indicating a poor sintering activity. The sintering process (>900 °C) can be divided into three typical stages: (i) the first shrinkage stage at 977–1318 °C; (ii) the second unique self-expansion stage at 1318–1495 °C; and (iii) the third re-shrinkage stage (1495–1550 °C). These were well discussed in the previous report.[11]

Because of MgO addition (2 wt.% and 4 wt.%), the sintering activity was obviously improved. On the one hand, the addition of MgO resulted in higher shrinkage in the high temperature

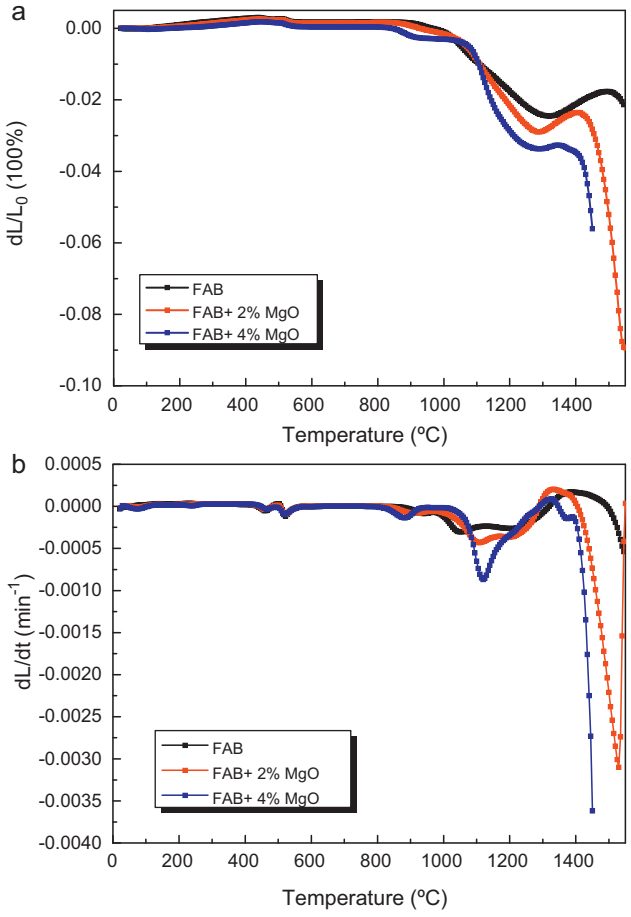

Fig. 1. (a) Linear shrinkage dL/L_0 and (b) differential linear shrinkage dL/dt of the flyash-based mullite samples with different magnesia contents.

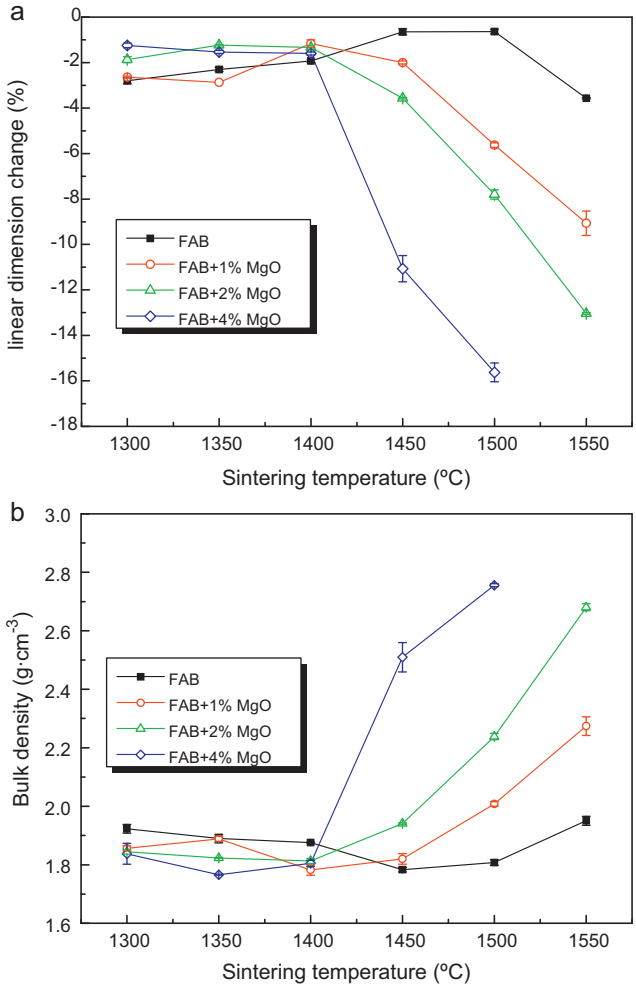

Fig. 2. (a) Linear dimensional changes and (b) bulk densities of the flyash-based mullite with various MgO contents after sintering at 1300–1500 °C for 2 h.

range, especially in the third stage (Fig. 1a). Basically, percentage sintering shrinkage increases as MgO content increases in the range of 0–4 wt.% in three different stages. With 2 wt.% MgO addition, the self-expansion stage starts at 1289 °C and extends to 1405 °C. Compared with the sample without MgO, the self-expansion stage of the 2 wt.% MgO doped sample is a much narrower range of temperature and shifts to a lower temperature region, indicating that densification was promoted. This change is more obvious for 4 wt.% MgO (self-expansion stage: 1290–1347 °C). The initial temperatures in the self-expansion stage are 1289 and 1290 °C for 2 wt.% and 4 wt.% MgO, which is lower than that of 0 wt.% MgO (1318 °C). With increasing magnesia content, the initial temperatures of the third re-shrinkage stages are also decreased, which are, respectively, 1495 °C, 1405 °C, and 1347 °C for 0, 2 and 4 wt.% magnesia. On the other hand, in the first shrinkage and third re-shrinkage stages, the samples with magnesia (2 wt.% and 4 wt.%) show much higher shrinkage rates (dL/dt) than that without magnesia (see Fig. 1b). The samples with magnesia achieved more rapid densification during the third re-densification stage, whereas the magnesia-free sample requires a little more time. This indicates the tremendous driving force for diffusion, which facilitated enhanced densification of the samples with addition of magnesia. But, in the expansion stage all three samples have similar shrinkage rates.

3.1.2. Linear dimension change and bulk density

Fig. 2 displays the linear dimensional changes (a) and bulk densities (b) as a function of sintering temperature, for the sintered mullite samples with different MgO contents. For 1 wt.% MgO, a gradual expansion in dimensions, associated with a continuous decrease in bulk density, is observed at 1300–1500 °C, suggesting a self-expansion process. From 1500 to 1550 °C, further shrinkage took place while the bulk density increases, indicating a re-densification process. Overall, the sample without MgO exhibits poor sinterability.

By comparison, the magnesia-containing samples exhibit slighter expansions (1300–1400 °C at 1 wt.% MgO, 1300–1350 °C at 2 wt.% MgO and around 1300 °C at 4 wt.% MgO) followed by rapid densification at higher temperatures. Above 1400 °C, with increasing magnesia content, linear shrinkage and bulk density increased, indicating that the addition of magnesia has a positive effect on densification. However, for 4 wt.% MgO, a further increase in temperature

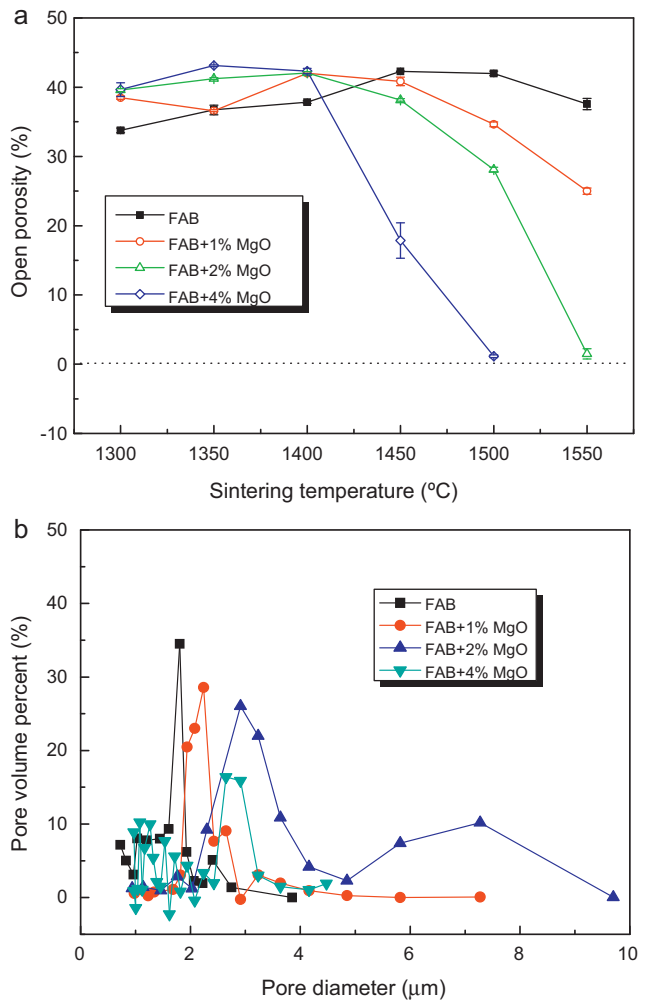

Fig. 3. (a) Open porosities of the flyash-based mullite with different MgO contents sintered at different temperatures and (b) pore size distributions of the flyash-based mullite with different MgO contents sintered at 1450 °C.

up to 1550 °C, led to visible bloating of the samples during the experiment.

3.1.3. Pore structure

Fig. 3 shows the variation in open porosity in relation to MgO content at different sintering temperatures (Fig. 3a) and the pore size distribution curves of the samples containing different magnesia contents after sintering at 1450 °C for 2 h (Fig. 3b). As shown in Fig. 3a, below 1400 °C, the porosities of the samples with magnesia are slightly higher than those without magnesia, which is ascribed to the sintering inhibition function of the newly formed periclase phase, derived from the decomposition of basic magnesium carbonate.[19] On the contrary, above 1400 °C, the samples show a rapidly decreasing porosity with increasing temperature, and also increasing MgO content, which is due to the occurrence of significant densification induced by an increase in the amount of formed magnesia-containing silica-rich ternary liquid phase ($MgO–Al_2O_3–SiO_2$). The sample containing 2 wt.% MgO shows an open porosity of $1.49 \pm 0.75\%$ at 1550 °C and the sample containing 4 wt.% MgO shows an open porosity of only $1.14 \pm 0.20\%$ at a lower temperature of 1500 °C. Therefore, at reduced temperatures, the porosity can be effectively decreased by addition of basic magnesium carbonate.

Fig. 3b shows the pore size distributions of the mullite samples sintered at 1450 °C for 2 h. From 0 to 2.0 wt.% (magnesia content), the average pore diameter firstly increases from 1.89 to 2.91 μm and the pore size distribution curve clearly broadens and shifts to larger pore sizes. On the one hand, fresh pores were formed because of the generation of gases such as CO_2 (from $MgCO_3$) and H_2O (from crystallization water and $Mg(OH)_2$) via the decomposition of ($(MgCO_3)_4·Mg(OH)_2·5H_2O$) below 400 °C.[20] Also, during further firing, the dehydroxylation of diaspore (AlO(OH)) and kaolinite ($Al_2O_3·2SiO_2·2H_2O$) in bauxite and the consequent combustion of residual carbon in flyash resulted in the production of new pores.[11,20,21] On the other hand, during viscous flow sintering at high temperature, due to the addition of magnesia, much more multiple oxide liquid phase was generated, resulting in the retardation of the pore elimination process. Therefore, large pores were formed, though the thickness difference of the measured samples has a slight effect on pore size according to the Hagen–Posieuille equation during the bubble-point test.[22] But, a slight decrease of average pore size is observed from 2.0 wt.% to 4.0 wt.% magnesia, indicating the penetration of liquid phase with low viscosity into the formed pores.

The above results support each other, sufficiently indicate that magnesia promoted the sintering of fly-ashed mullite. This can be ascribed to the formation of a metastable silica-rich liquid phase in the $Al_2O_3–SiO_2–MgO$ system with low viscosity at high temperatures, facilitating diffusion by lowering interfacial energy.[23] According to the $MgO–Al_2O_3–SiO_2$ ternary phase diagram, due to the presence of added MgO, the formation of a low-melting-point liquid phase was expected at a low peritectic temperature (1578 °C) for a composition in the corundum-mullite-spinel phase field.[24] Moreover, pre-existing impurities such as alkali metal oxides (even low Na_2O or K_2O level), alkaline earth metal oxides in raw material further reduced this peritectic temperature and promoted formation of significant levels of low melting point liquid phase.[25] During sintering, the formed ternary liquid phase accelerated mass transport via a dissolution–diffusion reprecipitation process, resulting in enhanced densification at relatively low temperatures.

3.2. Mechanical strength and microstructure

3.2.1. Mechanical strength

Fig. 4 shows the flexural strength of the flyash-based mullite samples as a function of magnesia content after sintering at selected temperatures. At 1300 °C, the flexural strength values are low at all contents of magnesia, but slightly increasing from 19.0 MPa at 0% MgO to 23.0–24.0 MPa at 1–4% magnesia. At 1450 °C, a significant increase in strength is observed, and increasing with magnesia content (especially from 0 to 2 wt.%). Flexural strengths are 27.16 ± 2.26, 34.71 ± 2.08, 40.28 ± 1.44 and 42.74 ± 1.28 MPa for samples with additions of 0, 1, 2 and 4 wt.% MgO. A similar trend between strength and mag-

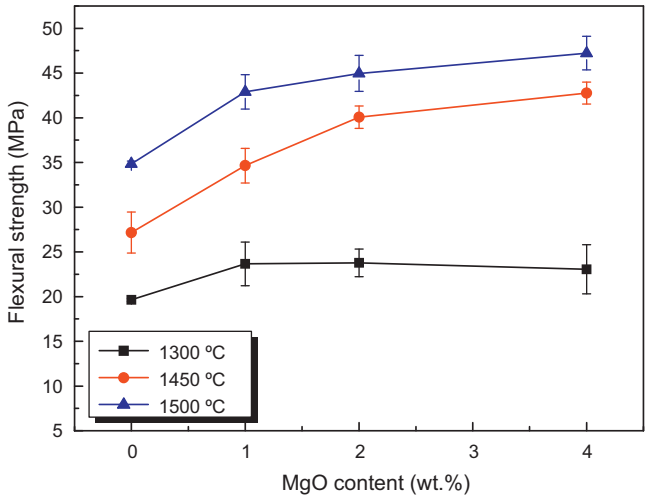

Fig. 4. The variation in three-point flexural strength with magnesia contents (0–4 wt.%) of flyash-based mullite sintered at various temperatures.

nesia content is observed at 1500 °C. It is clear that the addition of MgO results in an increase in strength, especially at higher sintering temperatures.

3.2.2. SEM and EDS analysis

Fig. 5 shows microstructural evolution by SEM of the fly-ash based mullite samples with 2 wt.% MgO sintered at 1300–1500 °C before and after FH etching. The microstructures are closely related to sintering temperature. At 1300 °C (Fig. 5a), a porous microstructure is observed, indicating a slight densification. On the one hand, from 1300 to 1500 °C, the samples exhibit more and more dense microstructures, associated also with increases in pore size and decrease of pore volume, which was suggested in the observed fractural surfaces before HF etching. Large pores were also observed during synthesis of porous mullite from kaolin and Mg powder.[26] On the other hand, sintering caused the growth of rod-like secondary mullite crystals. It is difficult to detect any mullite crystals at 1300 °C (Fig. 5b) but at 1400 °C, a large number of secondary mullite crystals with acicular shape have grown and are embedded in glassy phase (Fig. 5d). At 1500 °C, further growth of these elongated mullite crystals occurs and larger crystals are observed in an interlocking microstructure. It is well known that higher temperatures decrease the viscosity of the SiO_2-rich liquid phase, stimulating faster diffusion and reaction to form anisotropic mullite crystals.

Fig. 6 illustrates the SEM micrographs of the mullite with different MgO contents sintered at 1450 °C before and after HF etching. The addition of magnesia had a positive influence on densification of the samples (Fig. 6a, c and e), even at low magnesia content (e.g. 1 wt.%). From Fig. 6a, a porous microstructure is formed at 0 wt.% magnesia. At 1 wt.% magnesia, the sample is denser, containing a small number of pores (Fig. 6c). At 4 wt.% magnesia, a much denser microstructure was formed. Also, the morphology of mullite crystals depends largely on magnesia content. Very fine mullite crystals are observed at 0 wt.% magnesia. With increasing magnesia content (Fig. 6b, d and f), much more elongated mullite crystals with regular faceted boundaries are observed giving an interlocking microstructure, especially at 4 wt.% magnesia. Diffusion between added MgO and the high-energy but less stable surface regions of the mullite grains favours the formation of a liquid phase along the grain boundaries. Furthermore, during cooling, due to its partial crystallization, this type of liquid phase accelerates the growth of anisotropic rod-like mullite with boundaries parallel to {1 1 0} crystal planes because of low energy configurations.[27] Large mullite grains were developed due to inadequate growth sites in liquid phase.

Table 1
Average composition of the detected elements of the mullite crystals in the HF-etched samples without and with 4 wt.% MgO addition (Fig. 6).

	Element (in wt.%)		
	Mg	Al	Si
(without MgO, Fig. 6b)			
Spectrum-1	1.89	85.37	12.74
Spectrum-2	0.32	75.86	23.83
Spectrum-3	0.53	77.62	21.84
Spectrum-4	−0.63	80.70	19.93
(with 4 wt.% MgO, Fig. 6f)			
Spectrum-1	0.17	75.96	23.87
Spectrum-2	26.99	70.65	2.36
Spectrum-3	1.48	74.68	23.84
Spectrum-4	0.94	73.28	25.77

The mullite crystals in the samples without and with 4 wt.% MgO were analyzed by EDS (Table 1). For the sample without magnesia, average contents of Mg, Al and Si are 0.53 wt.%, 79.89 wt.% and 19.58 wt.%, respectively. In some locations, very high levels of Al were detected giving a ratio of Al to Si of about 4.08, which is much higher than that of stoichiometric mullite ($3Al_2O_3{\cdot}2SiO_2$), i.e., 2.88. This is because the excessive growth of mullite nuclei through liquid phase caused the entrapment of bauxite-derived alumina within mullite crystals. This is similar to other result.[28] At 4 wt.% MgO, the micro-region marked as spectrum-2 (Fig. 6f) has a high Mg content (26.99 wt.%) and a low Si content (2.36 wt.%). The Al:Mg ratio is 2.62, that is close to that of the $MgAl_2O_4$ spinel of 2.25. Combining with the following XRD results, it is concluded that this micro-region is $MgAl_2O_4$ spinel. For three other spectra, they are slightly richer in magnesia compared with the sample without magnesia and it may be concluded that magnesium enters into the crystal lattice of mullite to form a solid solution.

Based on the above microstructural analysis, two factors are considered as the main reasons for the improvement in strength after magnesia addition: (1) both magnesia addition and high temperature produced high densities; (2) the microstructure of large compact interlocked rod-like mullite crystals is the result of magnesia addition. On experiencing a grain boundary fracture, the area of fracture was increased and cracks absorbed much more energy. As a result, interlocked elongated mullite crystals could increase the fracture energy and corresponding high flexural strengths are observed.

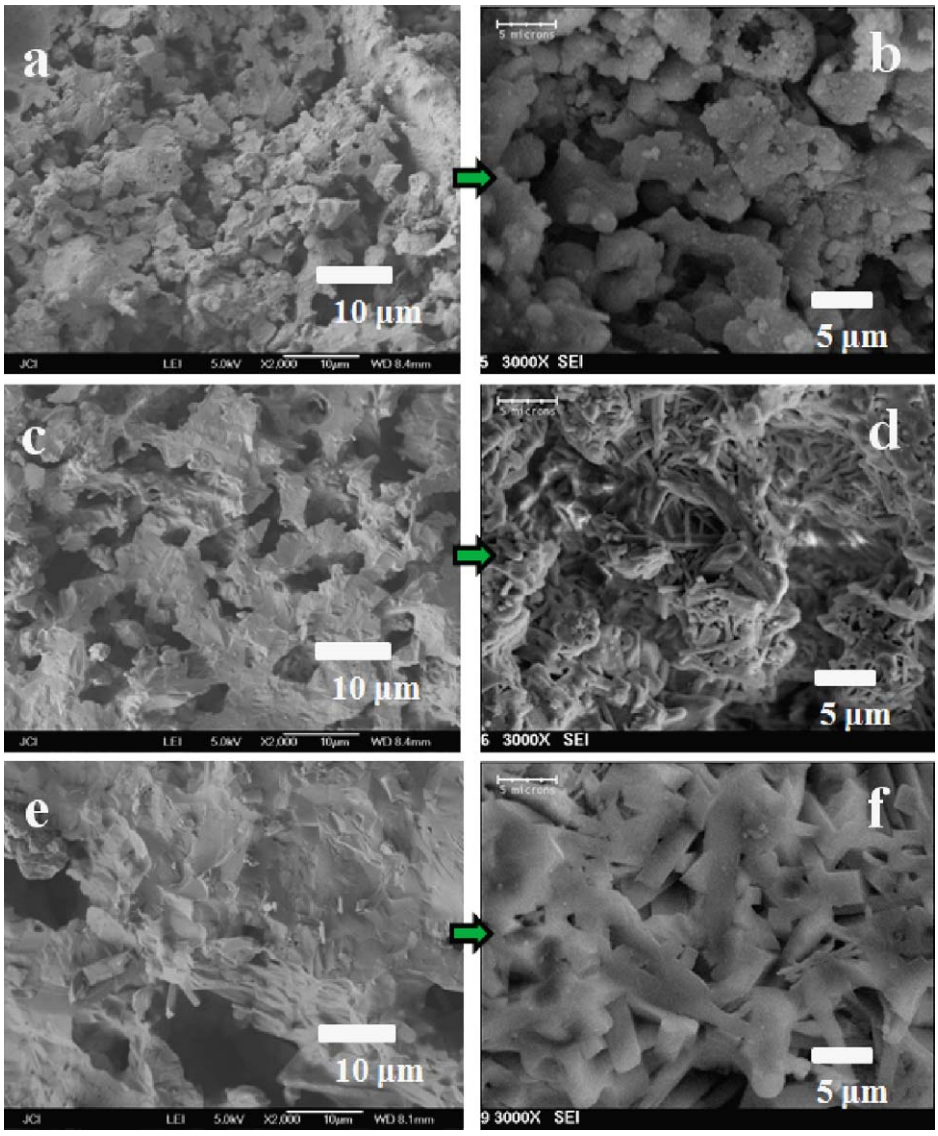

Fig. 5. SEM micrographs of fracture surfaces of the mineral-based mullite samples with 2 wt.% MgO addition sintered at different temperatures for 2 h, before and after 15 vol% HF solution etching for 20 min: (a) 1300 °C before etching, (b) 1300 °C after etching, (c) 1400 °C before etching, (d) 1400 °C after etching, (e) 1500 °C before etching, and (f) 1500 °C after etching.

3.3. Thermal expansion and phase analysis

3.3.1. Thermal expansion coefficient

Fig. 7 displays the linear thermal expansion coefficients (LTEC) of the mullite with different magnesia contents after sintering at 1300–1500 °C. The relationships between LTEC and magnesia content show different trends at different sintering temperatures. At 1300 °C, the addition of magnesia slightly decreases the LTEC. At 1400 °C, 1450 °C and 1500 °C, however, the addition of magnesia slightly increases the LTEC.

3.3.2. XRD analysis

Fig. 8 shows the XRD patterns of the mullite samples with 0–4 wt.% MgO sintered at 1300–1500 °C. At 0 wt.% MgO (Fig. 8a), from 1300 to 1450 °C, the peak intensity of corundum gradually decreases and almost approaches zero at 1450 °C because it dissolves into a transient liquid phase for the further secondary mullitization reaction.[29,30] Above 1450 °C mullite is the only crystalline phase. For 1 wt.% MgO (Fig. 8b), at 1300 °C, besides mullite and α-alumina, α-cordierite was also detected. At 1400 °C, α-cordierite disappears because it decomposes to form mullite crystals and a magnesia-rich liquid phase. Corundum phase appears at 1300 and 1400 °C, then disappears above 1400 °C due to mullitization reaction. Over 1400–1500 °C, mullite is the only crystalline phase. At 2 wt.% MgO (Fig. 8c), besides mullite and α-alumina, α-cordierite appears at 1300 and 1350 °C, and then disappears at 1400 °C. From 1300 to 1350 °C, the peak intensity of corundum phase gradually decreases because of its dissolution for secondary mullitization, but it increases slightly at 1400 °C and is still detected at 1400–1500 °C. According to the $MgO–Al_2O_3–SiO_2$ phase diagram, due to the addition of magnesia, a liquid with higher silica and lower alumina than 3:2 mullite is formed, which results in formation of α-alumina during cooling under non-equilibrium

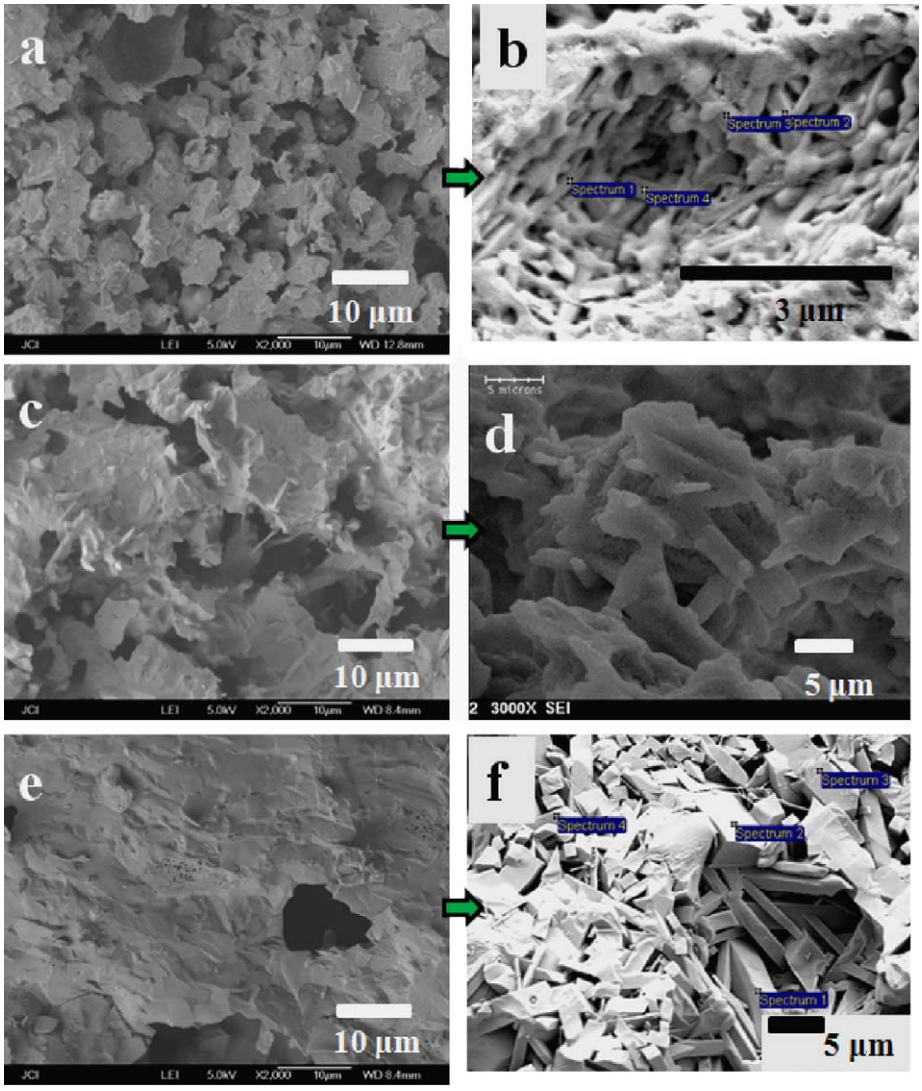

Fig. 6. SEM micrographs of fracture surfaces of flyash-based mullite samples with various MgO contents sintered at 1450 °C for 2 h, before and after 15 vol% HF solution etching for 20 min: (a) 0 wt.% MgO before etching, (b) 0 wt.% MgO after etching, (c) 1 wt.% MgO before etching, (d) 1 wt.% MgO after etching, (e) 4 wt.% MgO before etching, and (f) 4 wt.% MgO after etching.

conditions. At 4 wt.% MgO, high content α-cordierite is detected at 1300 °C. The peak intensity of corundum decreases from 1300 to 1350 °C, but then increases from 1400 to 1500 °C. At 1500 °C, corundum and mullite were detected as major phases with $MgAl_2O_4$ spinel as a minor phase. It can be understood from the $MgO–Al_2O_3–SiO_2$ phase diagram that, due to magnesia addition, $MgAl_2O_4$ spinel crystals are formed as a result of devitrification of the magnesia-containing aluminum silicate liquid by a solution-reprecipitation process during cooling.[15] Above the peritectic point, mullite, α-alumina and liquid phase are expected to be formed. Below the peritectic point, mullite, spinel and liquid should be present. Therefore, under cooling, non-equilibrium presence of mullite, α-alumina and spinel occurred.

The LTEC changes can be correlated with phase composition. At 1300 °C, the slight decrease in LTEC is due to the formation of α-cordierite with low LTEC ($1.0–2.0 \times 10^{-6}\ K^{-1}$ at 25–1000 °C). The slight increases in LTEC at 1400–1500 °C

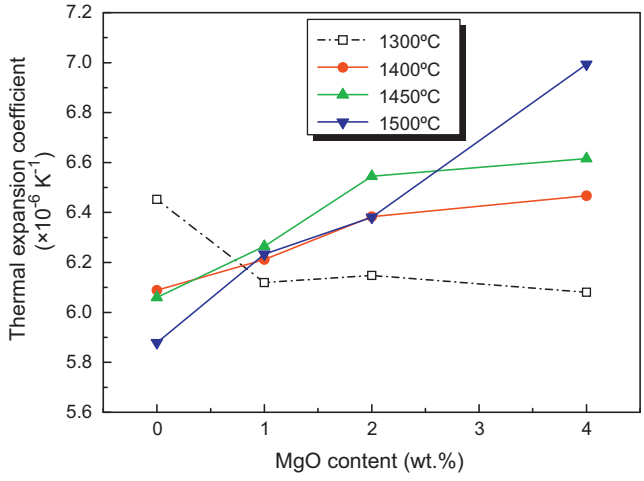

Fig. 7. Linear thermal expansion coefficients of flyash-based mullite with different magnesia contents after sintering at various temperatures.

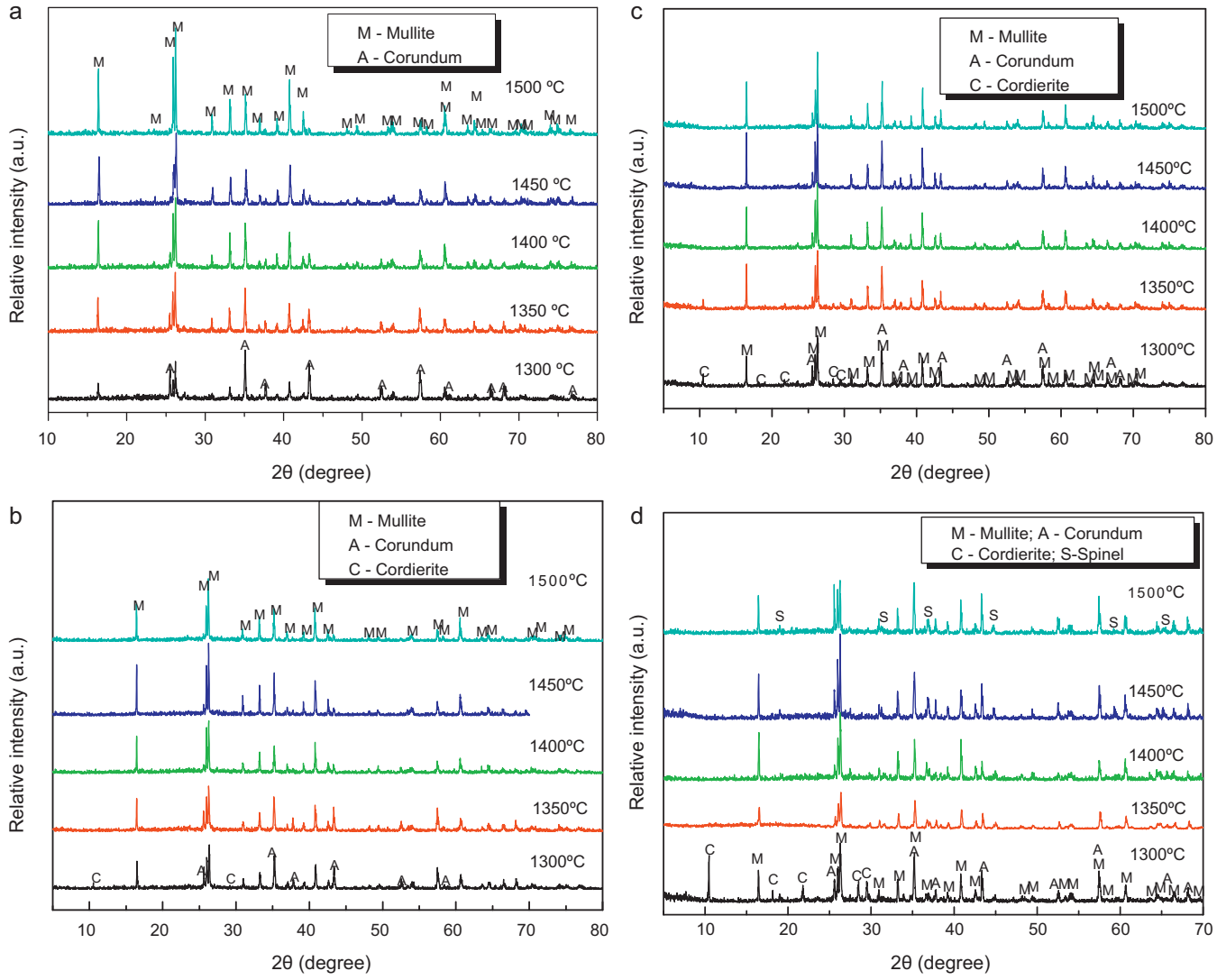

Fig. 8. XRD patterns of the flyash-based mullite samples sintered at various temperatures for 2 h: (a) without MgO, (b) with 1 wt.% MgO, (c) 2 wt.% MgO and (d) 4 wt.% MgO.

are ascribed to the existence of high expansion phases: $MgAl_2O_4$ spinel ($8.9 \times 10^{-6}\,K^{-1}$ at 200–1000 °C) and corundum ($8.8 \times 10^{-6}\,K^{-1}$ at 200–1000 °C), and the consumption of low expansion quartz glass ($0.5 \times 10^{-6}\,K^{-1}$ at 200–1000 °C) for precipitation and growth of mullite crystals.

4. Conclusions

This research has investigated sintering of mullite made from recycled flyash and natural bauxite with MgO additions. The following conclusions can be drawn:

(1) The sintering process of the flyash/bauxite mixture can be divided into three stages: (i) the first shrinkage stage at 977–1318 °C; (ii) the second self-expansion stage at 1318–1495 °C; and (iii) the third re-shrinkage stage (1495–1550 °C).
(2) MgO additions to the flyash/bauxite mixture promote densification by decreasing volume expansion, especially at higher temperatures during the second stage. The results of shrinkage, bulk density and pore structure effectively confirm the sintering aid function of magnesia which allows the formation of a magnesia-containing silica-rich ternary liquid phase.
(3) Due to the presence of large interlocking elongated mullite crystals, associated with good densification of the samples, an improvement in strength is obtained for mullite samples containing magnesia, especially sintered higher than 1400 °C. The addition of magnesia slightly decreases the LTEC at 1300 °C due to the formation of low-expansion α-cordierite, but slightly increases the LTEC at temperatures higher than 1400 °C due to the formation of high expansion corundum and $MgAl_2O_4$ spinel.

Acknowledgements

The authors wish to thank the Irish Research Council for Science, Engineering and Technology (IRCSET) through an

EMPOWER Post-doctoral Research Fellowship (YD) and China Post-Doctoral Grant (contract no. 20100470846) for financial supports.

References

1. Mukherjee AB, Zevenhoven R, Bhattacharya P, Sajwan KS, Kikuchi R. Mercury flow via coal and coal utilization by-products: a global perspective. *Resour Conserv Recycl* 2008;**52**:571–91.
2. Manz OE. Worldwide production of coal ash and utilization in concrete and other products. *Fuel* 1997;**76**:691–6.
3. Ahmaruzzaman M. A review on the utilization of fly ash. *Prog Energy Combust Sci* 2010;**36**:327–63.
4. Hulett Jr LD, Weinberger AJ, Northcutt KJ, Fergusone M. Chemical species in fly ash from coal-burning power plants. *Science* 1980;**210**:1356–8.
5. Sarin P, Yoon W, Haggerty RP, Chiritescu C, Bhorkar NC, Kriven WM. Effect of transition-metal-ion doping on high temperature thermal expansion of 3:2 mullite—an in situ, high temperature, synchrotron diffraction study. *J Eur Ceram Soc* 2008;**28**:353–65.
6. Sarkar A, Rano R, Udaybhanu G, Basu AK. A comprehensive characterisation of fly ash from a thermal power plant in Eastern India. *Fuel Process Technol* 2006;**87**:259–77.
7. Huang X. Properties of mullite synthesized from fly ash and alumina mixture. *Fuel Energy Abstr* 1996;**37**:49–149.
8. Huang X, Hwang JY, Mutsuddy BC. Properties of mullite synthesized from fly ash and alumina mixture. *Ceram Int* 1995;**44**:65–165.
9. Hwang JY, Huang X, Hein AM. Synthesizing mullite from beneficiated fly ash. *J Met* 1994;**465**:36–9.
10. Jung JS, Park HC, Stevens R. Mullite ceramics derived from coal fly ash. *J Mater Sci Lett* 2001;**20**:1089–91.
11. Dong YC, Feng XY, Feng XF, Ding YW, Liu XQ, Meng GY. Preparation of low-cost mullite ceramics from natural bauxite and industrial waste fly ash. *J Alloys Compd* 2008;**460**:599–606.
12. Doni Jayaseelan D, Amutha Rani D, Benny Anburaj D, Ohji T. Pulse electric current sintering and microstructure of industrial mullite in the presence of sintering aids. *Ceram Int* 2004;**30**:539–43.
13. Kim YW, Kim HD, Park CB. Processing of microcellular mullite. *J Am Ceram Soc* 2005;**88**:3311–5.
14. Imose M, Ohta A, Takano Y, Yoshinaka M, Hirota K, Yamaguchi O. Low-temperature sintering of mullite/yttria-doped zirconia composites in the mullite-rich region. *J Am Ceram Soc* 1998;**81**:1050–2.
15. Montanaro L, Perrot C, Esnouf C, Thollet G, Fantozzi G, o Negro A. Sintering of industrial mullites in the presence of magnesia as a sintering aid. *J Am Ceram Soc* 2000;**83**:189–96.
16. Montanaro L, Tulliani JM, Perrot C, Negro A. Sintering of industrial mullites. *J Eur Ceram Soc* 1997;**17**:1715–23.
17. Gopi Chandran R, Chandrashekar BK, Ganguly C, Patil KC. Sintering and microstructural investigations on combustion processed mullite. *J Eur Ceram Soc* 1996;**16**:843–9.
18. Venkataraman K, Choate WT, Torre ER, Husung RD, Batchu HR. Characterization studies of ceramic membranes. A novel technique using a Coulter® Porometer. *J Membr Sci* 1988;**39**:259–71.
19. Dong YC, Liu XQ, Ma QL, Meng GY. Preparation of cordierite-based porous ceramic micro-filtration membranes using waste fly ash asthe main raw materials. *J Membr Sci* 2006;**285**(1/2):173–81.
20. Kloprogge JT, Ruan HD, Frost RL. Thermal decomposition of bauxite minerals: infrared emission spectroscopy of gibbsite. Boehmite and diaspore. *J Mater Sci* 2002;**37**:1121–9.
21. Abou-Sekkina MM, Abo-El-Enein SA, Khalil NM, Shalma OA. Phase composition of bauxite-based refractory castables. *Ceram Int* 2010;**37**:411–8.
22. Jakobs E, Koros WJ. Ceramic membrane characterization via the bubble point technique. *J Membr Sci* 1997;**124**:149–59.
23. Sacks MD, Pask JA. Sintering of mullite-containing materials: effect of composition. *J Am Ceram Soc* 1982;**65**:65–70.
24. Phase equilibrium diagrams of oxide systems, Plate 3, American Ceramic Society and Edward Orton Jr, Ceramic Foundation, 160.
25. Chesters JH. *Refractories: production and properties*. Inst of Materials; 1983.
26. Esharghawi A, Penot C, Nardou F. Contribution to porous mullite synthesis from clays by adding Al and Mg powders. *J Eur Ceram Soc* 2009;**29**: 31–8.
27. Kleebe HJ, Hilz G, Ziegler G. Transmission electron microscopy and electron energy-loss spectroscopy characterization of glass phase in sol–gel-derived mullite. *J Am Ceram Soc* 1996;**79**:2592–600.
28. She JH, Mechnich P, Schmücker M, Schneider H. Low-temperature reaction-sintering of mullite ceramics with an Y_2O_3 addition. *Ceram Int* 2001;**27**:847–52.
29. Chen CY, Lan GS, Tuan WH. Preparation of mullite by the reaction sintering of kaolinite and alumina. *J Eur Ceram Soc* 2000;**20**:2519–25.
30. Sainz MA, Serrano FJ, Amigo JM, Bastida J, Caballero A. XRD microstructural analysis of mullites obtained from kaolinite-alumina mixtures. *J Eur Ceram Soc* 2000;**20**:403–12.